crystals

MDPI

Supporting Materials

To be or not to be a (4,4) net: Reactions of 4'-{4-(*N*,*N*-diethylaminophenyl)}- and 4'-{4-(*N*,*N*-diphenylaminophenyl)}-3,2':6',3"- and 4,2':6',4"-terpyridines with cobalt(II) thiocyanate

Dalila Rocco, Anamarija Nikoletić, Alessandro Prescimone, Edwin C. Constable, Catherine E. Housecroft*

Department of Chemistry, University of Basel, Mattenstrasse 24a, BPR 1096, 4058 Basel, Switzerland

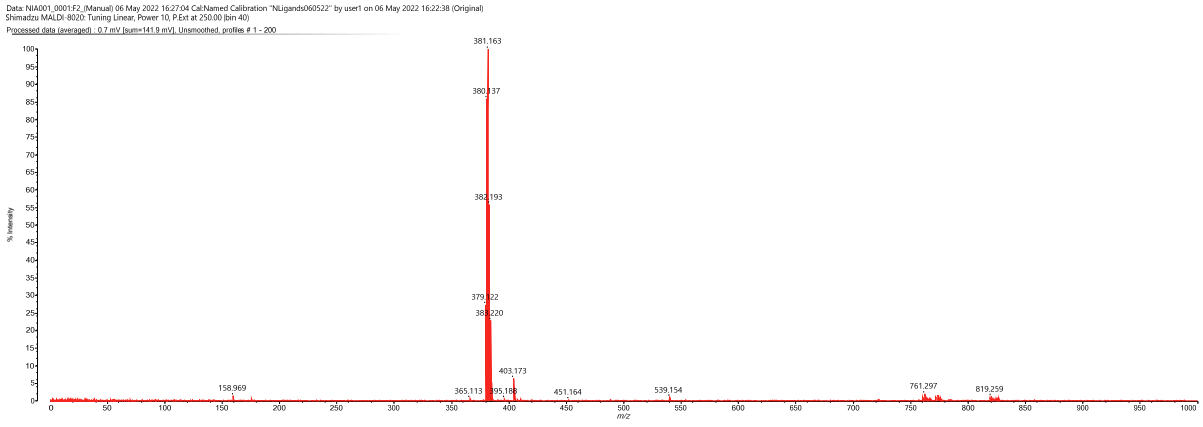

Figure S1. MALDI mass spectrum of **1**.

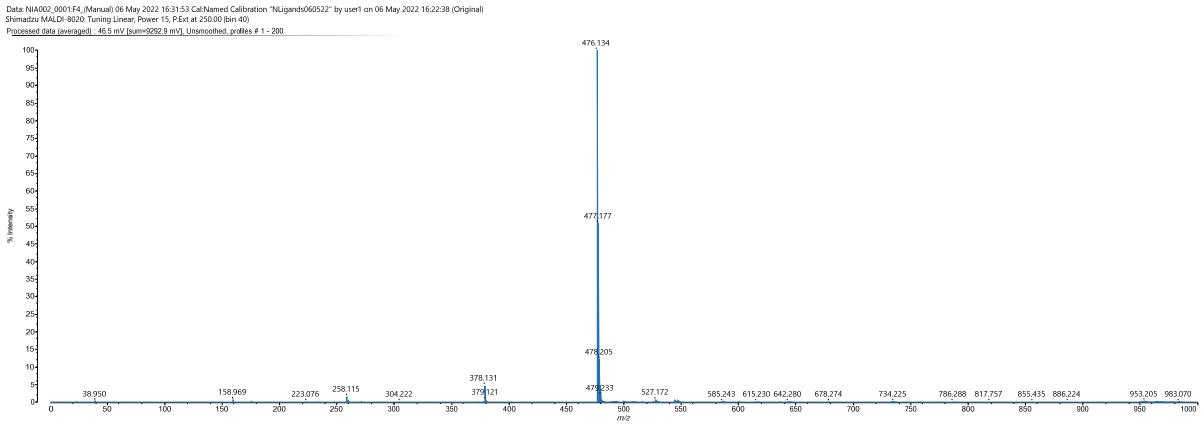

Figure S2. MALDI mass spectrum of **2**.

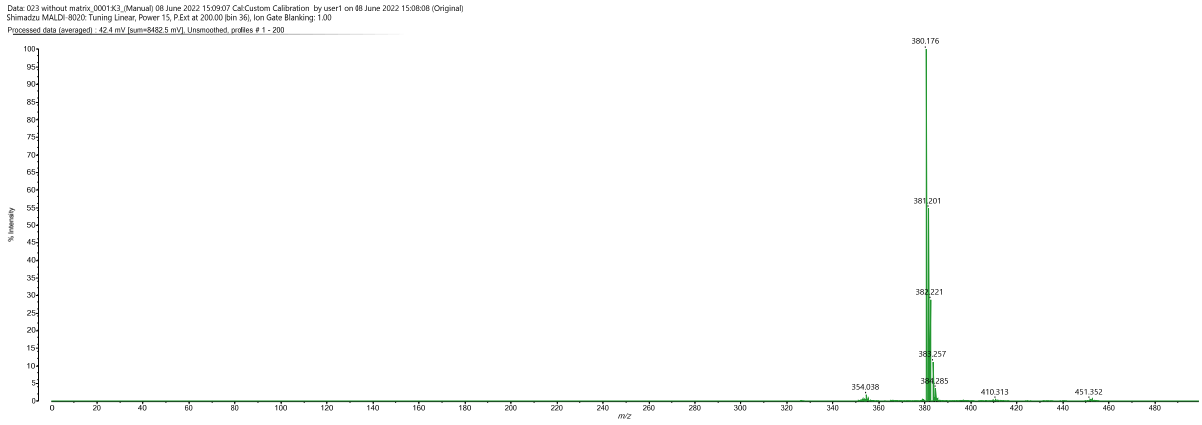

Figure S3. MALDI mass spectrum of **3**.

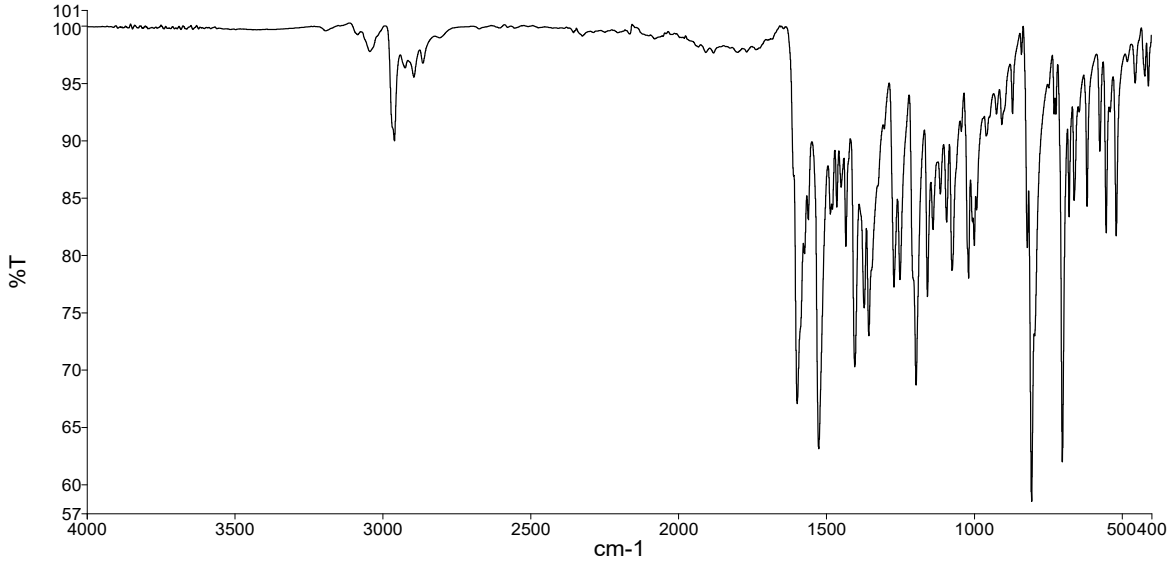

Figure S4. Solid-state IR spectrum of **1**.

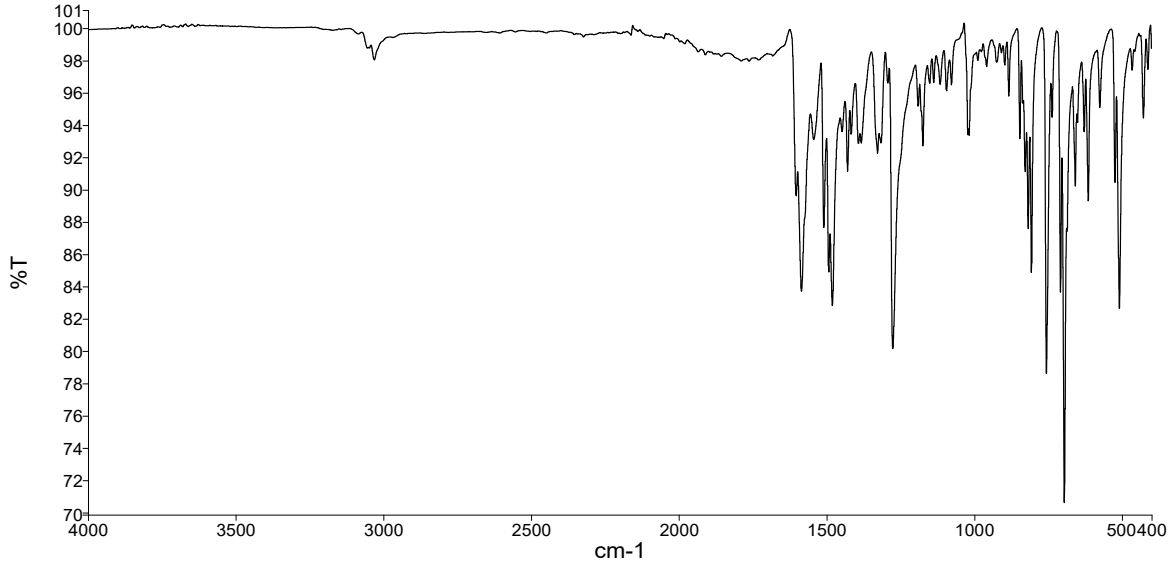

Figure S5. Solid-state IR spectrum of **2**.

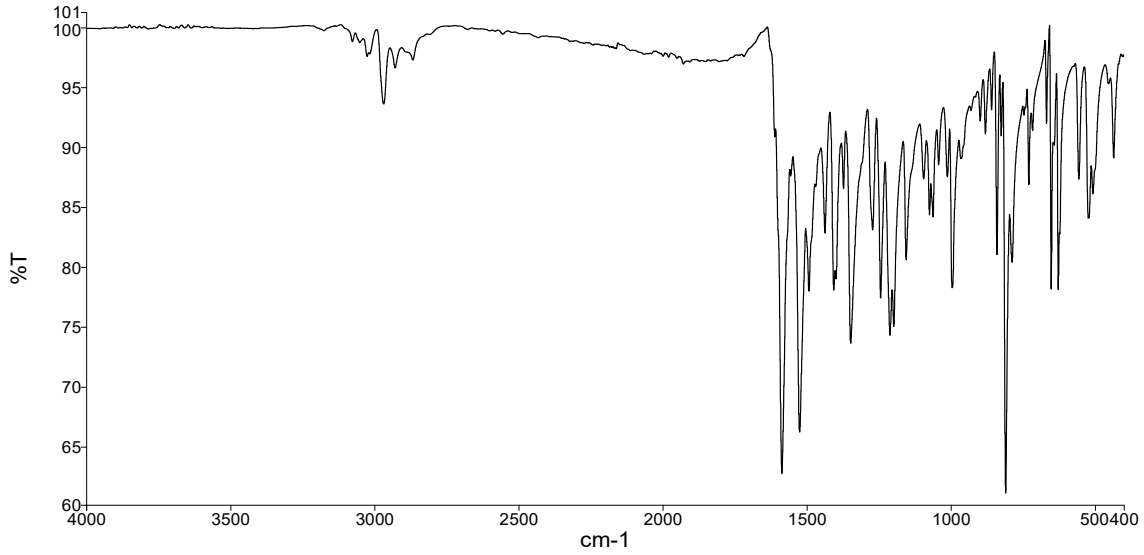

Figure S6. Solid-state IR spectrum of **3**.

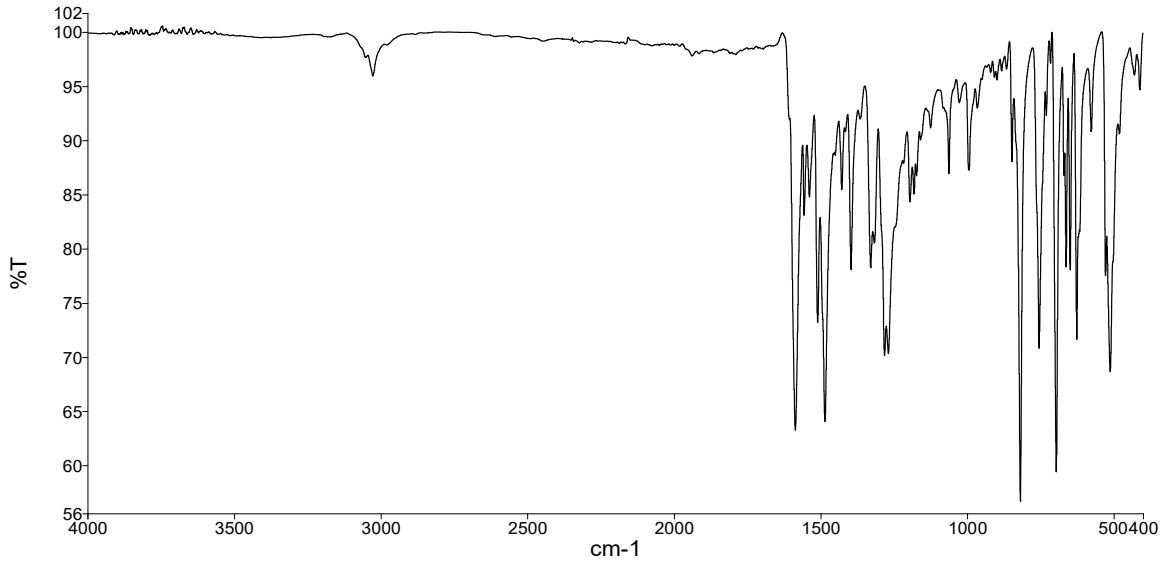

Figure S7. Solid-state IR spectrum of **4**.

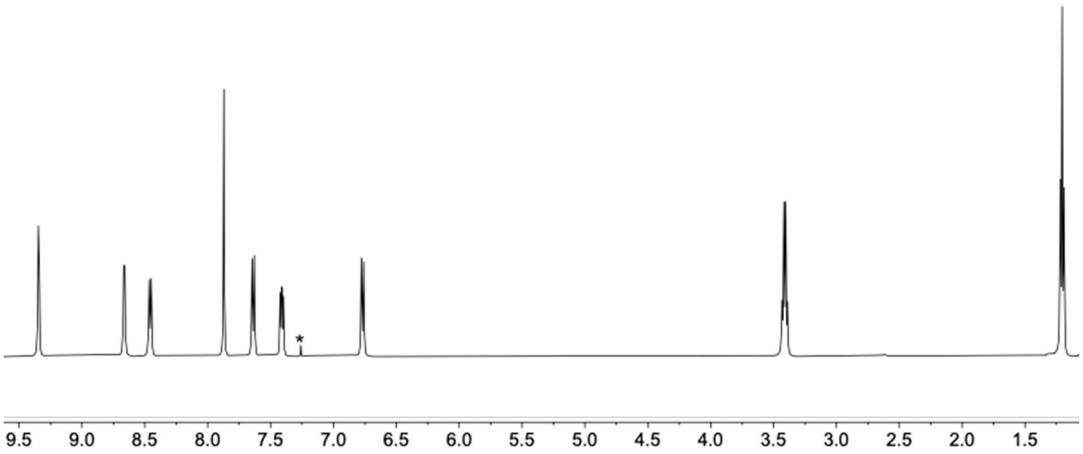

Figure S8. ^{1}H NMR spectrum of **1** (500 MHz, 298 K, $CDCl_3$). * = residual $CHCl_3$. Scale: δ/ ppm.

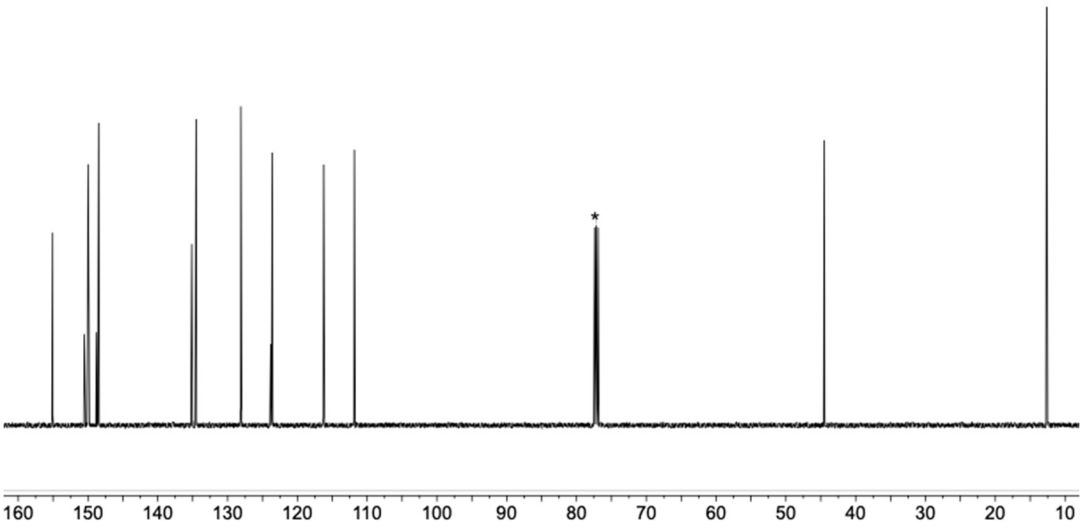

Figure S9. $^{13}C\{^{1}H\}$ NMR spectrum of **1** (126 MHz, 298 K, $CDCl_3$). * = $CDCl_3$. Scale: δ/ ppm.

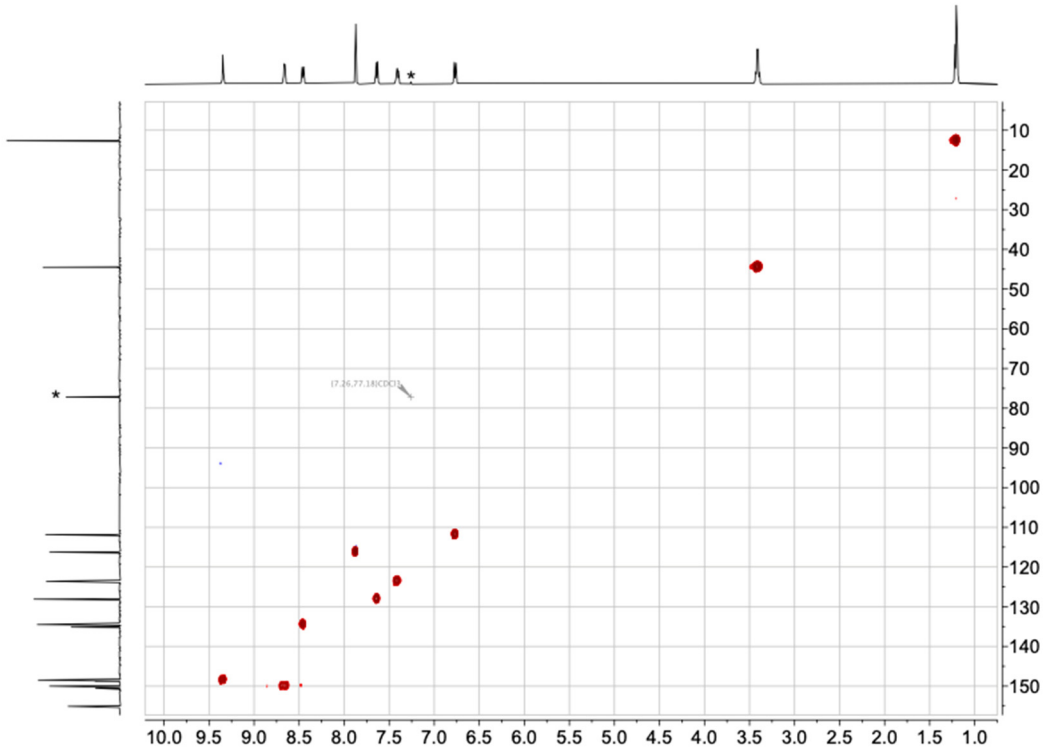

Figure S10. HMQC spectrum of **1** (500 MHz ^{1}H, 126 MHz ^{13}C{^{1}H}, 298 K, $CDCl_3$). * = residual $CHCl_3$ (^{1}H) or $CDCl_3$ (^{13}C). Scale: δ/ ppm.

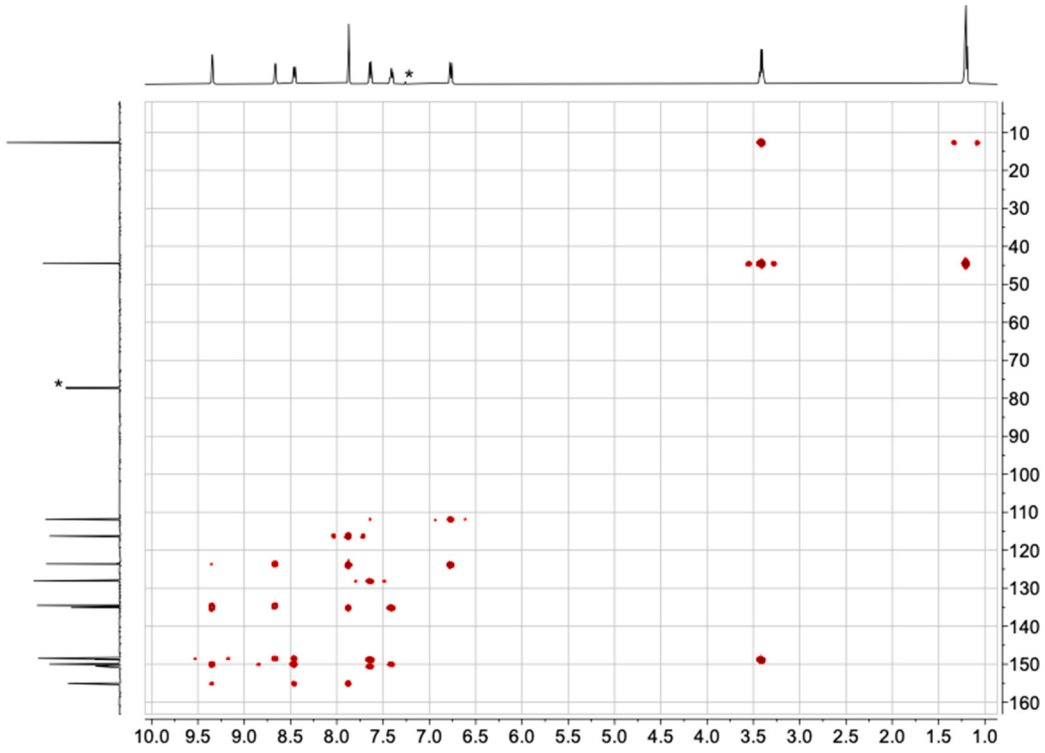

Figure S11. HMBC spectrum of **1** (500 MHz ^{1}H, 126 MHz ^{13}C{^{1}H}, 298 K, $CDCl_3$). * = residual $CHCl_3$ (^{1}H) or $CDCl_3$ (^{13}C). Scale: δ/ ppm.

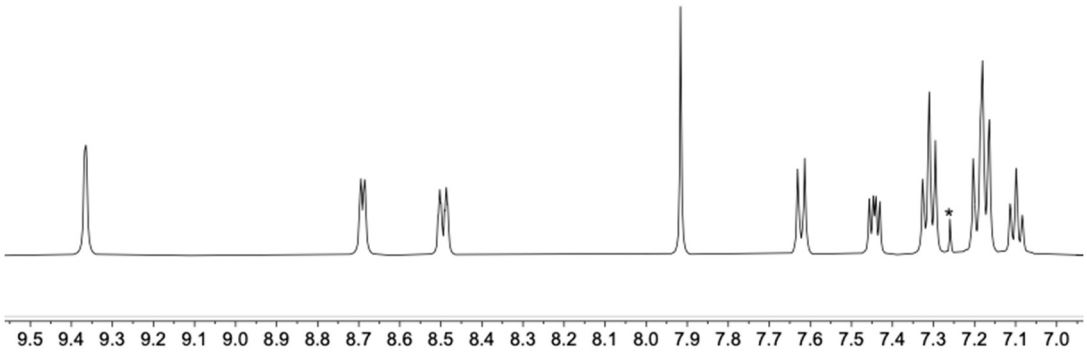

Figure S12. ^{1}H NMR spectrum of **2** (500 MHz, 298 K, $CDCl_3$). * = residual $CHCl_3$. Scale: δ/ ppm.

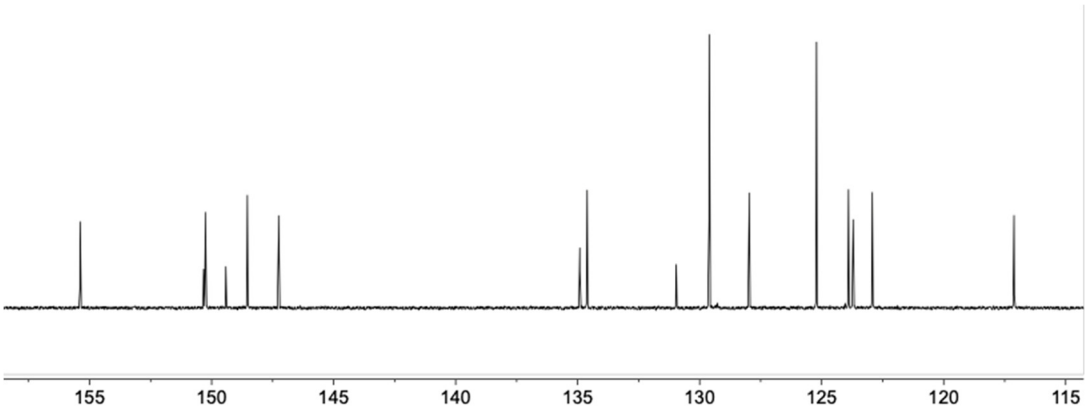

Figure S13. ^{13}C{^{1}H} NMR spectrum of **2** (126 MHz, 298 K, $CDCl_3$). * = $CDCl_3$. Scale: δ/ ppm.

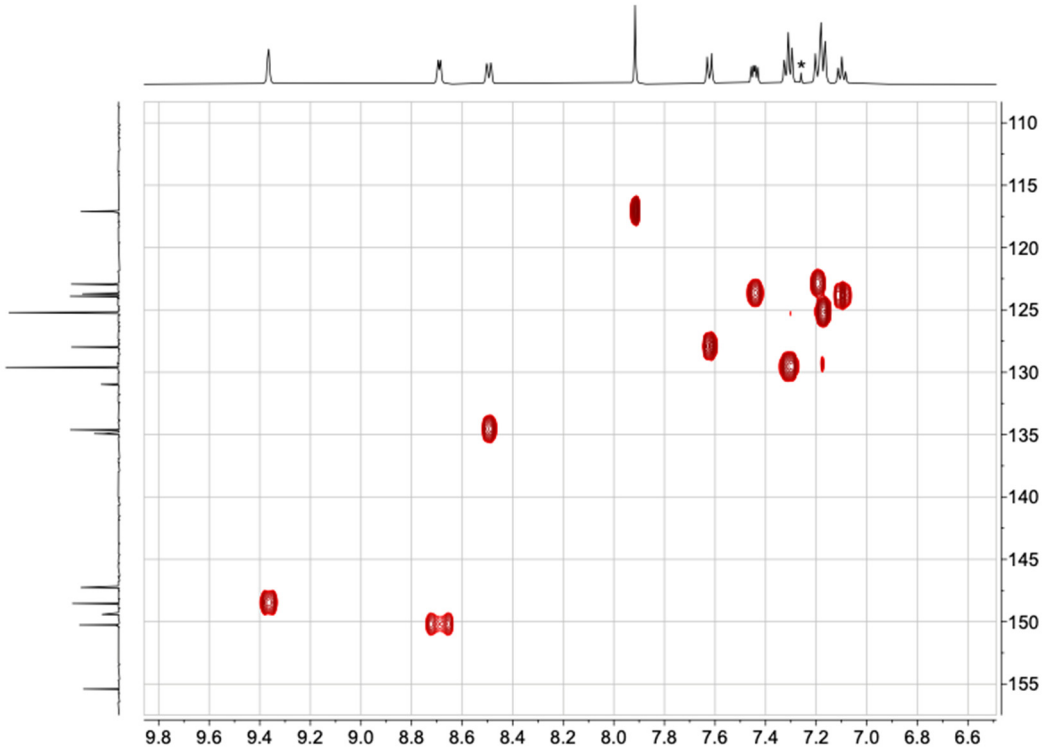

Figure S14. HMQC spectrum of **2** (500 MHz ^{1}H, 126 MHz ^{13}C{^{1}H}, 298 K, $CDCl_3$). * = residual $CHCl_3$. Scale: δ/ ppm.

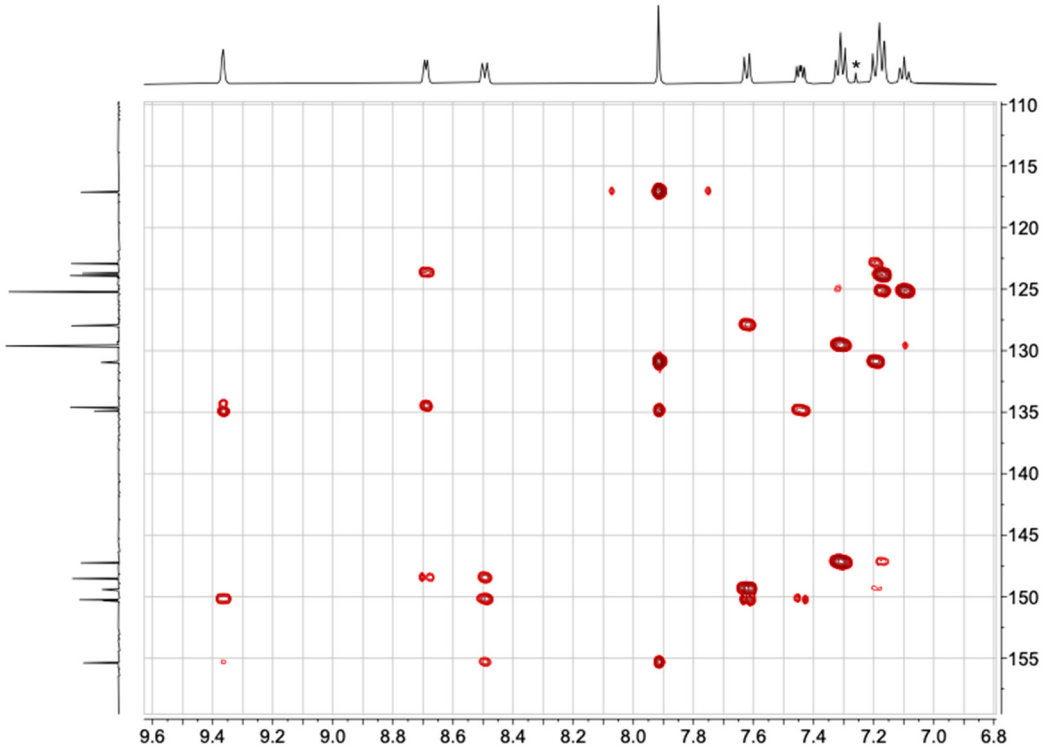

Figure S15. HMBC spectrum of **2** (500 MHz ^{1}H, 126 MHz ^{13}C{^{1}H}, 298 K, $CDCl_3$). * = residual $CHCl_3$. Scale: δ/ ppm.

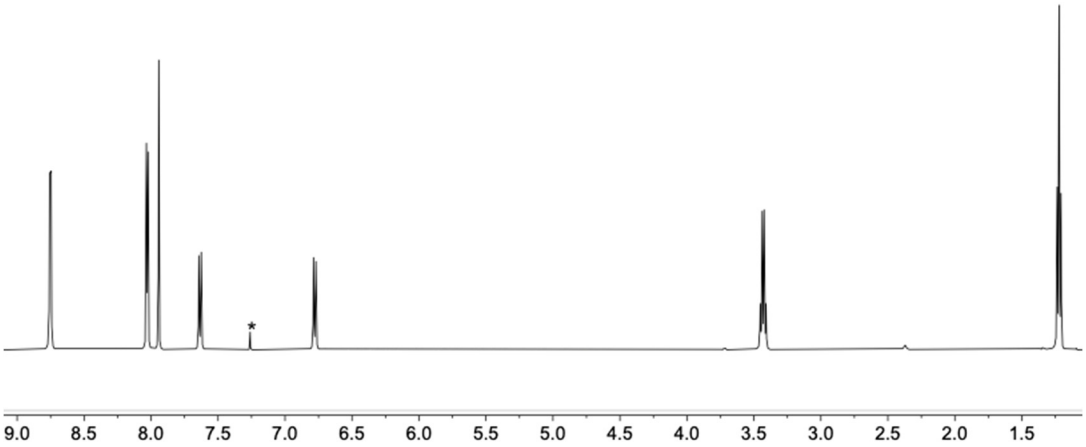

Figure S16. ^{1}H NMR spectrum of **3** (500 MHz, 298 K, $CDCl_3$). * = residual $CHCl_3$. Scale: δ/ ppm.

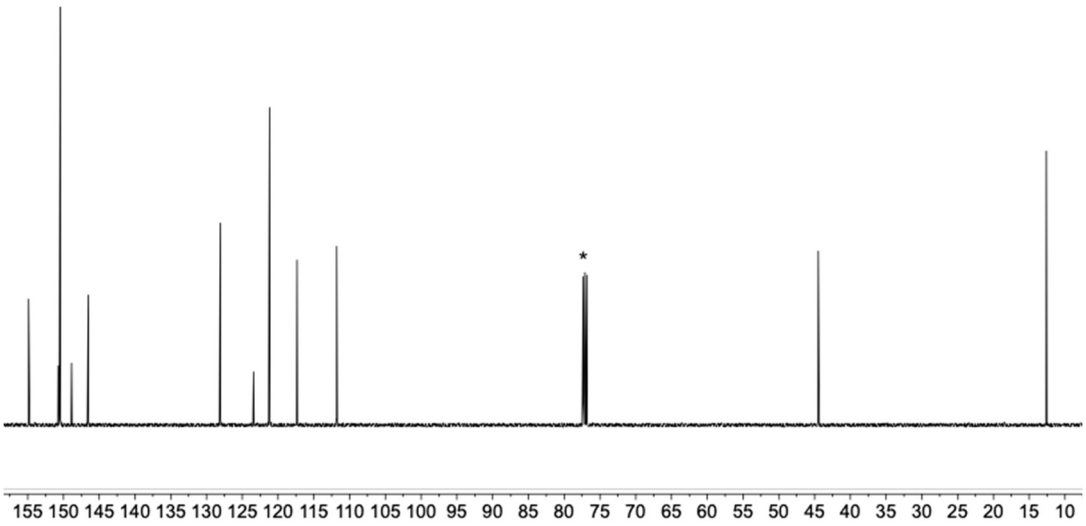

Figure S17. $^{13}C\{^{1}H\}$ NMR spectrum of **3** (126 MHz, 298 K, $CDCl_3$). * = $CDCl_3$. Scale: δ/ ppm.

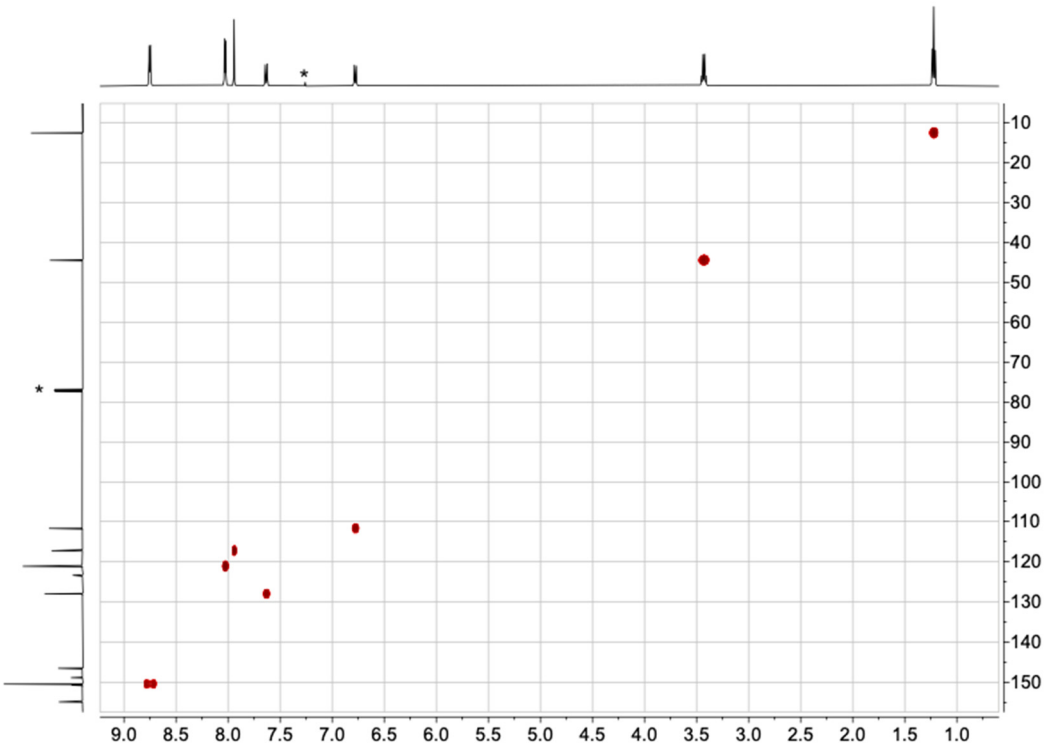

Figure S18. HMQC spectrum of **3** (500 MHz ^{1}H, 126 MHz ^{13}C{^{1}H}, 298 K, $CDCl_3$). * = residual $CHCl_3$ (^{1}H) or $CDCl_3$ (^{13}C). Scale: δ/ ppm.

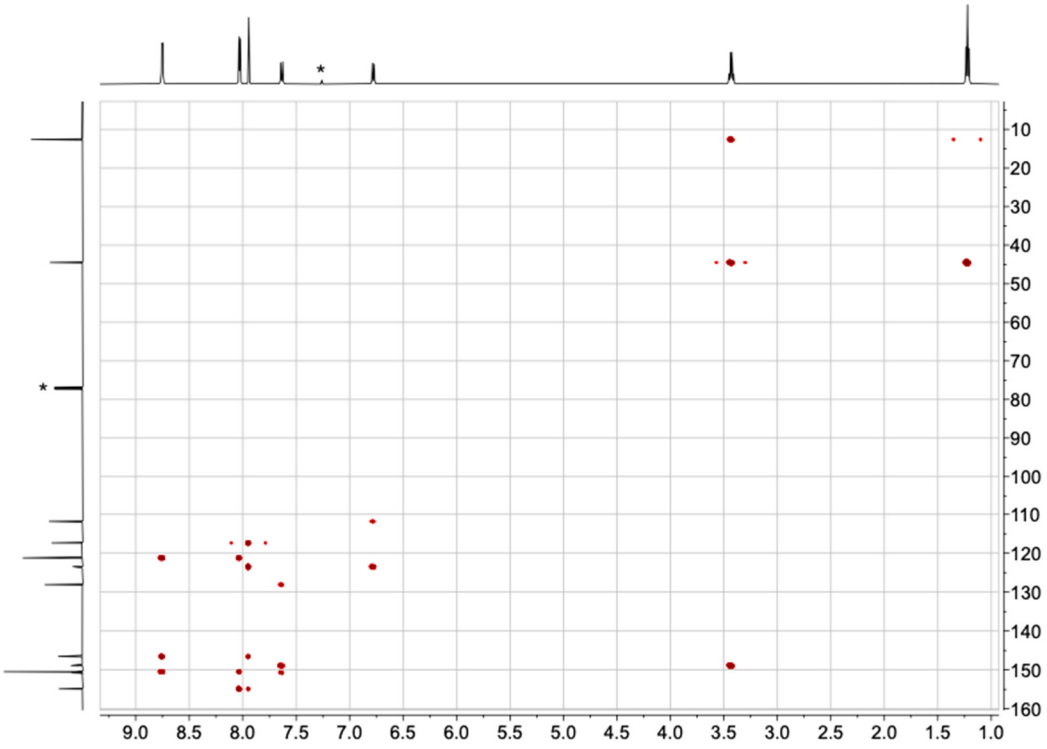

Figure S19. HMBC spectrum of **3** (500 MHz ^{1}H, 126 MHz ^{13}C{^{1}H}, 298 K, $CDCl_3$). * = residual $CHCl_3$ (^{1}H) or $CDCl_3$ (^{13}C). Scale: δ/ ppm.

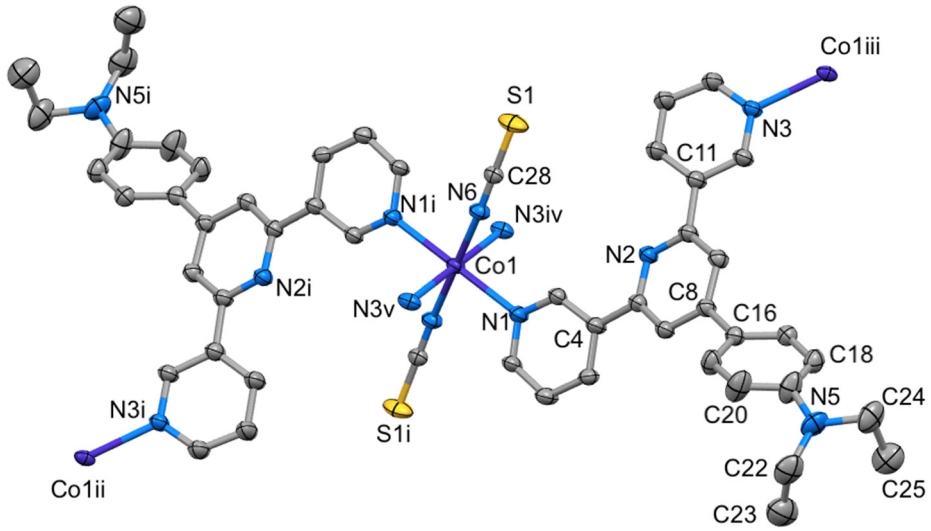

Figure S20. Structure of the asymmetric unit in $[Co(NCS)_2(\mathbf{1})]_n \cdot 0.8n CHCl_3$ with symmetry generated atoms. Ellipsoids are plotted at the 40% probability level. Solvent molecules and H atoms are omitted for clarity. The ring containing N1 and the NEt_2 unit are disordered and only the major occupancy sites are shown. Symmetry codes: i = $-x$, 2$-y$, 1$-z$; ii = $-{}^{1}/_{2}-x$, ${}^{1}/_{2}+y$, ${}^{1}/_{2}-z$; iii = ${}^{1}/_{2}-x$, $-{}^{1}/_{2}+y$, ${}^{3}/_{2}-z$; iv = ${}^{1}/_{2}-x$, ${}^{1}/_{2}+y$, ${}^{3}/_{2}-z$; v = $-{}^{1}/_{2}+x$, ${}^{3}/_{2}-y$, $-{}^{1}/_{2}+z$.

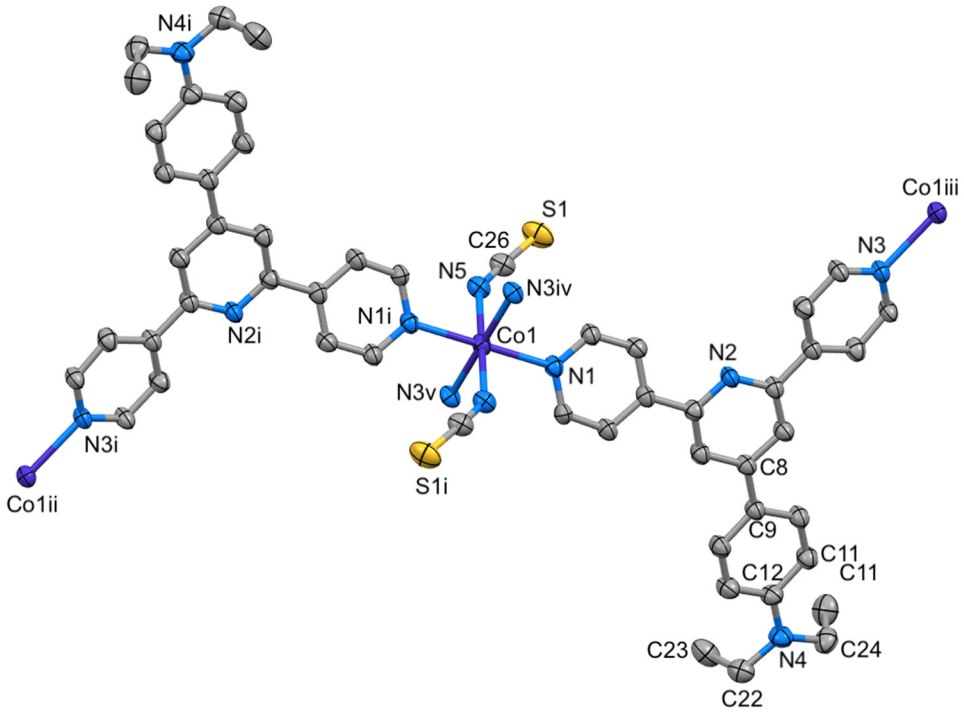

Figure S21. Structure of the asymmetric unit in $[Co(NCS)_2(\mathbf{3})]_n \cdot 2n CHCl_3$ with symmetry generated atoms. Ellipsoids are plotted at the 40% probability level. Solvent molecules and H atoms are omitted for clarity. Symmetry codes: i = 2–*x*, 2–*y*, 1–*z*; ii = $^3/_2$–*x*, $^1/_2$+*y*, $^1/_2$–*z*; iii = $^5/_2$–*x*, –$^1/_2$+*y*, $^3/_2$–*z*; iv = $^5/_2$–*x*, $^1/_2$+*y*, $^3/_2$–*z*; v = –$^1/_2$+*x*, $^3/_2$–*y*, –$^1/_2$+*z*.

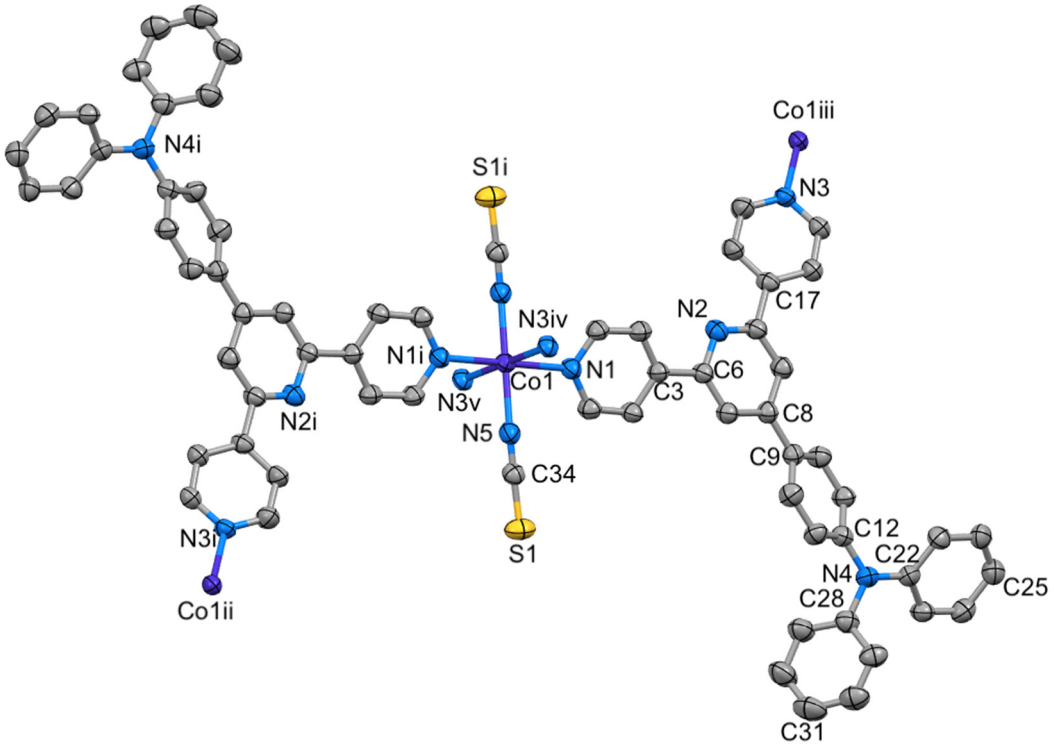

Figure S22. Structure of the asymmetric unit in $[Co(NCS)_2(\mathbf{4})]_n$ with symmetry generated atoms. Ellipsoids are plotted at the 40% probability level, and H atoms are omitted for clarity. Symmetry codes: i = 1–*x*, 1–*y*, 1–*z*; ii = 1–*x*, $-^1/_2$+*y*, $^1/_2$–*z*; iii = 1–*x*, $^1/_2$+*y*, $^3/_2$–*z*; iv = *x*, $^3/_2$–*y*, $-^1/_2$+*z*; v = 1–*x*, $-^1/_2$–*y*, $^3/_2$+*z*

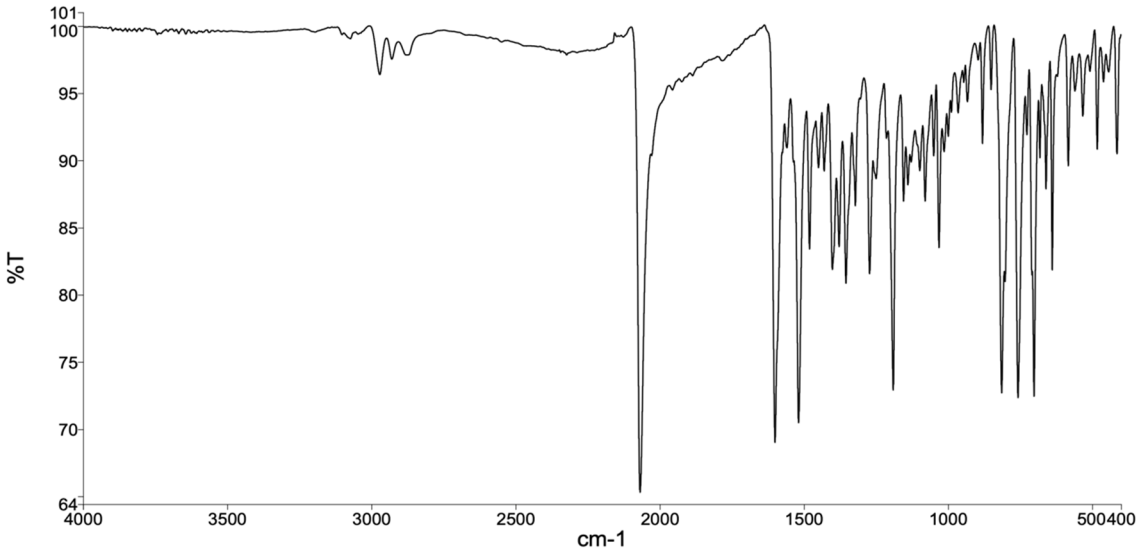

Figure S23. Solid-state FT-IR spectrum of the bulk sample of $[Co(NCS)_2(\mathbf{1})]_n$·0.8*n*$CHCl_3$.

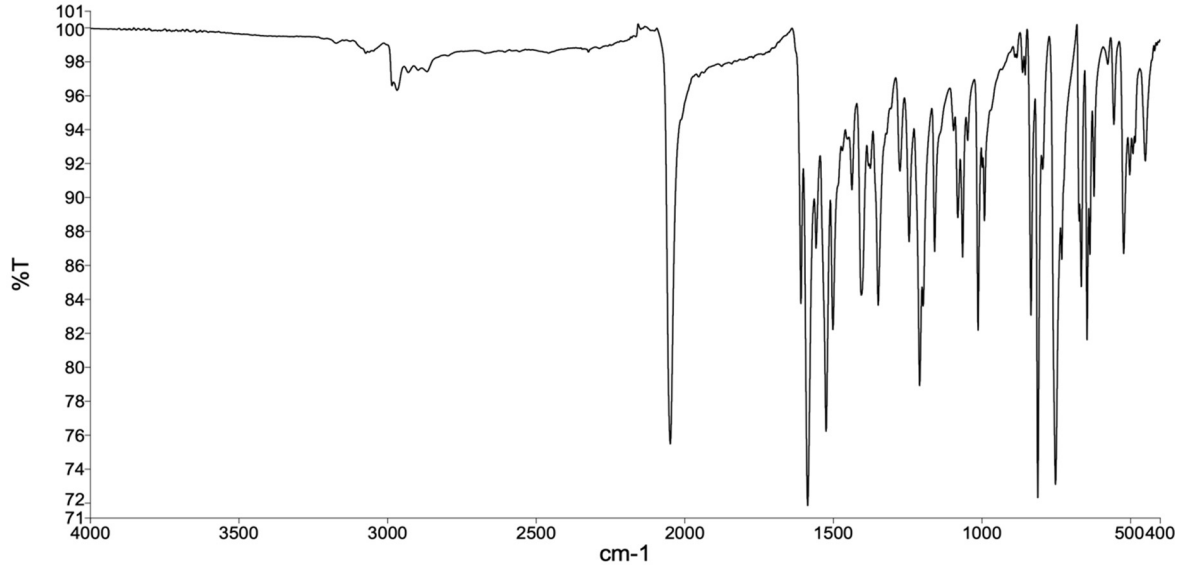

Figure S24. Solid-state FT-IR spectrum of the bulk sample of $[Co(NCS)_2(\mathbf{3})]_n 2n CHCl_3$.

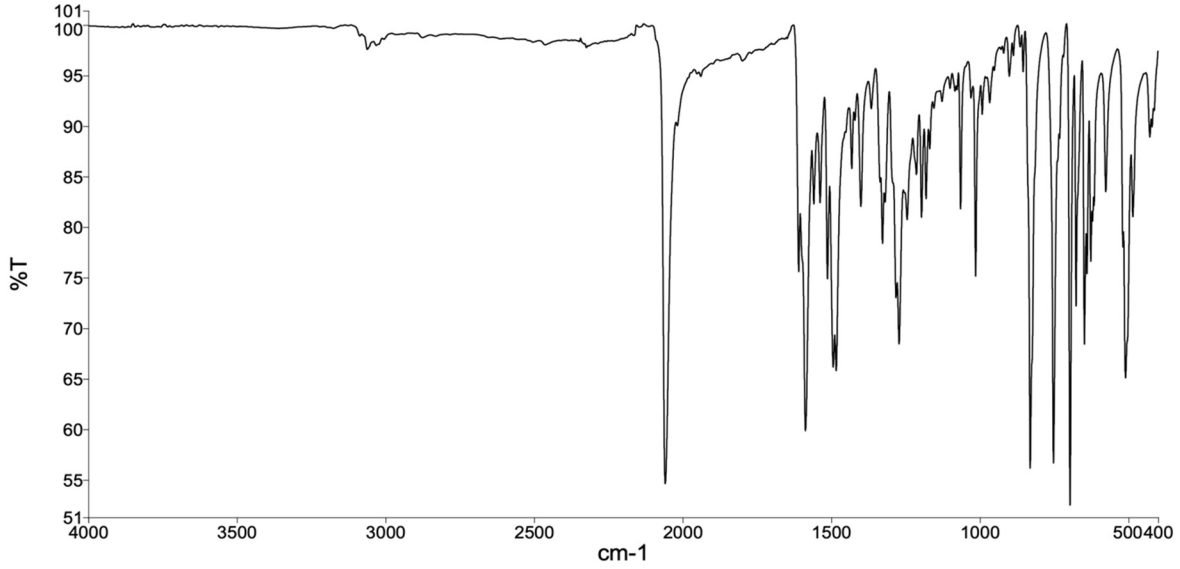

Figure S25. Solid-state FT-IR spectrum of the bulk sample of $[Co(NCS)_2(\mathbf{4})]_n$.

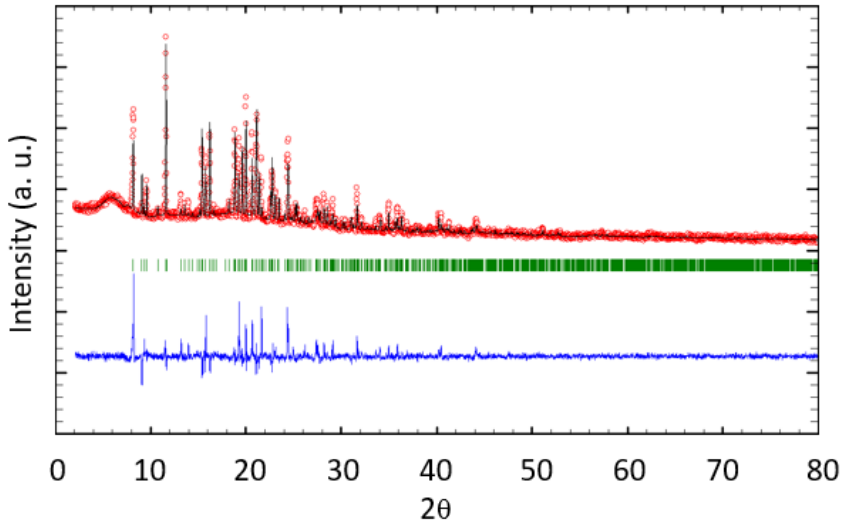

Figure S26. PXRD (CuKα1 radiation) patterns for [Co(NCS)$_2$(**1**)]$_n$·0.8nCHCl$_3$. The experimental data (red circles) are compared with the best fit from the Rietveld refinement analysis (black line). Bragg peak positions (green) and differences between the calculated and experimental plots (blue) are also displayed.

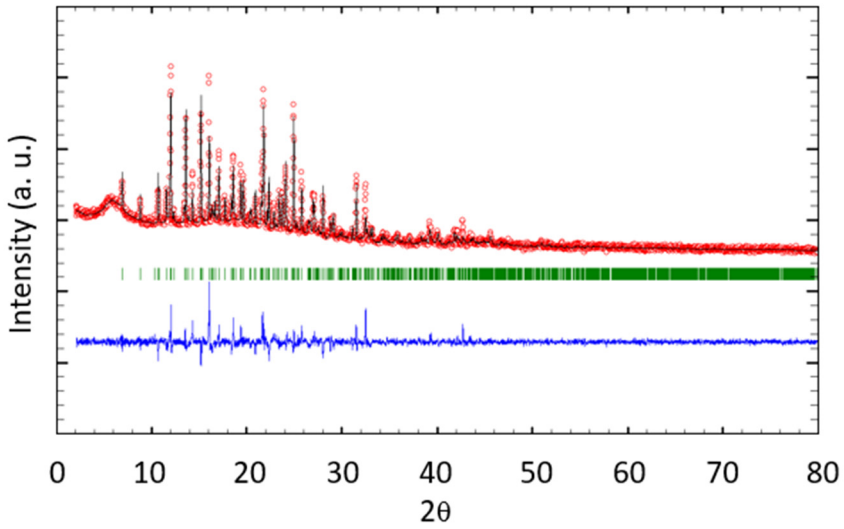

Figure S27. PXRD (CuKα1 radiation) patterns for [Co(NCS)$_2$(**3**)]$_n$2nCHCl$_3$. The experimental data (red circles) are compared with the best fit from the Rietveld refinement analysis (black line). Bragg peak positions (green) and differences between the calculated and experimental plots (blue) are also displayed.

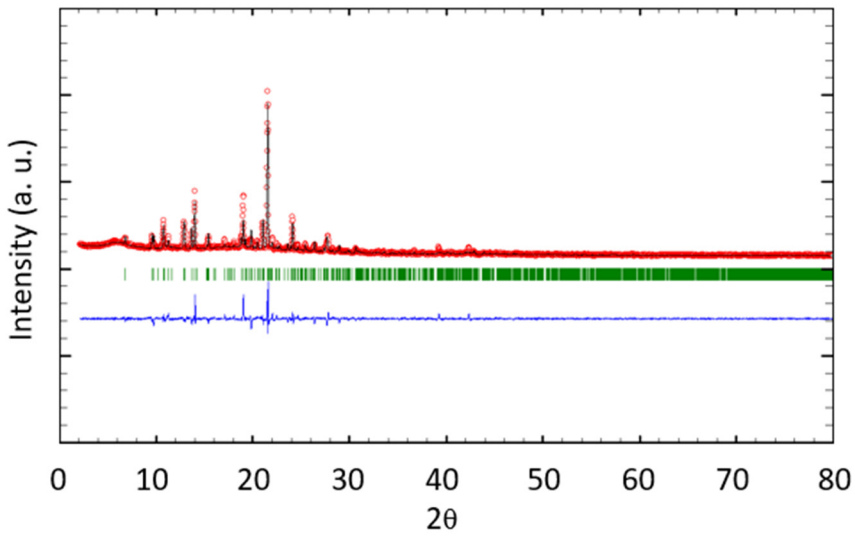

Figure S28. PXRD (CuKα1 radiation) patterns for [Co(NCS)$_2$(**4**)]$_n$. The experimental data (red circles) are compared with the best fit from the Rietveld refinement analysis (black line). Bragg peak positions (green) and differences between the calculated and experimental plots (blue) are also shown.

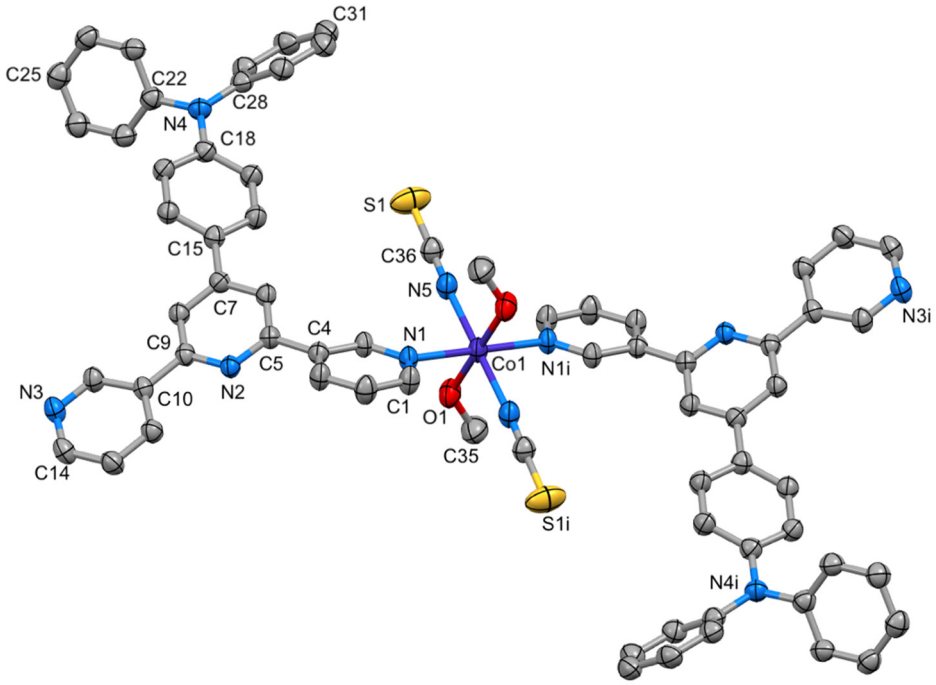

Figure S29. Structure of [Co(NCS)$_2$(**2**)$_2$(MeOH)$_2$]·3CHCl$_3$ with solvent molecules omitted. H atoms are also omitted for clarity. Ellipsoids are plotted at a 40% probability level. Symmetry code i = 2–*x*, –*y*, 1–*z*.

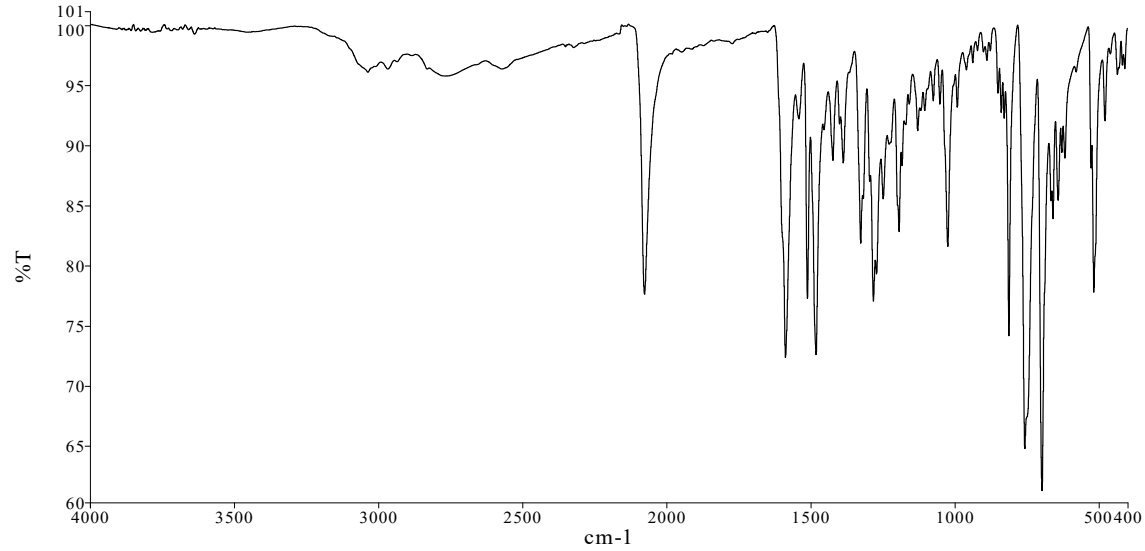

Figure S30. Solid-state FT-IR spectrum of the bulk sample of [Co(NCS)$_2$(**2**)$_2$(MeOH)$_2$]·3CHCl$_3$.

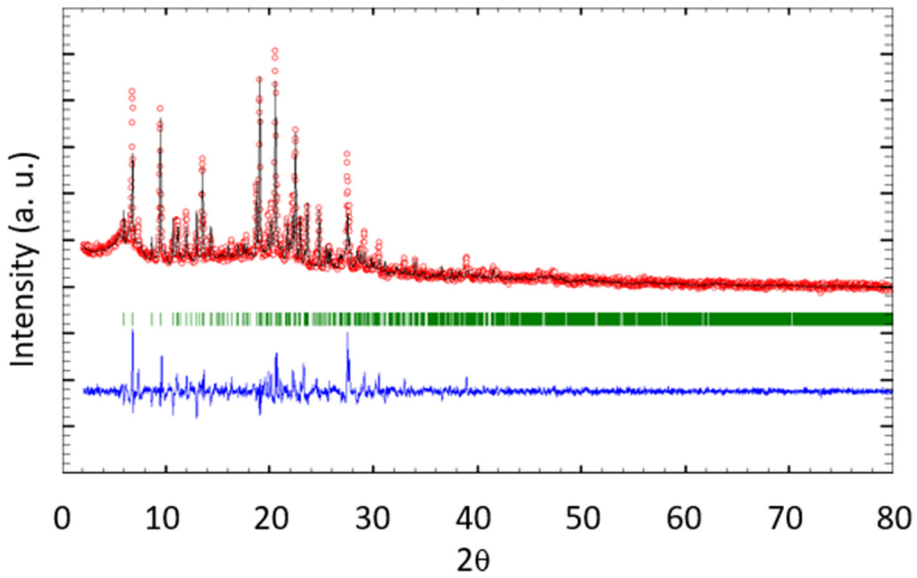

Figure S31. PXRD (CuKα1 radiation) patterns for [Co(NCS)$_2$(**2**)$_2$(MeOH)$_2$]·3CHCl$_3$. The experimental data (red circles) are matched to the best fit from the Rietveld refinement analysis (black line). Bragg peak positions (green) and differences between the calculated and experimental plots (blue) are also shown.